

# R245fa vertical downward flow boiling heat transfer characteristics in a micro/nano-porous surface coating tube

Shuang CAO<sup>1</sup>, He LIU<sup>1</sup>, Chunxia HU<sup>1\*</sup>, Xishi LI<sup>2</sup>, Zhanying ZHANG<sup>3</sup>

<sup>1</sup> School of Energy and Power Engineering, Zhengzhou University of Light Industry, Zhengzhou 450002, China

<sup>2</sup> Henan Refrigeration Society, Zhengzhou 450000, Henan, China

<sup>3</sup> School of Computer Science and Technology, Zhengzhou University of Light Industry, Zhengzhou 450002, China

\*Corresponding Author: Chunxia Hu. Email: 2002055@zzuli.edu.cn

*This research employed a combination of sintering and electrochemical deposition methods to prepare a micro/nano-porous coating on the inner wall of stainless-steel tube with an inner diameter of 10 mm. A vertical downward flow boiling experiment was conducted using R245fa as the working fluid to compare the flow boiling heat transfer characteristics between the smooth tube and the enhanced tube. The experimental parameters were as follows: the saturation pressure was maintained at 0.6 MPa, mass fluxes ranged from 200 to 700 kg/(m<sup>2</sup>s), heat fluxes varied from 5 to 75 kW/m<sup>2</sup>, and inlet vapor qualities spanned from 0 to 1. The findings indicated that both tubes exhibited only annular flow and dryness under the vertically downward flow conditions. The mass fluxes had a limited effect on heat transfer performance. However, as the inlet vapor quality increased, the boiling heat transfer coefficients exhibited a tendency to increase and then decrease, with the heat transfer coefficients of the enhanced tube outperforming those of the smooth tube. This phenomenon can primarily be attributed to the increased density of nucleation sites and superior surface wettability compared to that of the smooth tube. The enhancement factor for heat transfer and the performance evaluation coefficient achieved values of 1.884 and 1.762, respectively.*

*Key words: R245fa; Flow boiling; vertical downward flow; Heat transfer performance*

## 1 Introduction

Organic working fluid is widely used in the fields of waste heat recovery, heat pumps, air conditioning, and refrigeration systems. As one of the core components of the above system, evaporator plays a vital role in improving energy efficiency. Boiling heat transfer of organic working fluid in evaporator is a hot topic in recent years [1,2].

R245fa was considered an excellent organic working fluid due to its favorable combination of environmental friendliness and thermodynamic properties [3]. Over the past few years, scholars have conducted in-depth research on the boiling heat transfer performance of R245fa in flat flow direction to further explore its potential in industrial applications [4-7]. Al-Hajri et al. [8] conducted experimental studies on flow boiling heat transfer in microchannels using R134a and R245fa. The saturation temperatures ranged from 30°C to 70°C, and mass fluxes varying between 50-500 kg/(m<sup>2</sup>s). The experimental results showed that R245fa has a 25% higher heat transfer performance than R134a on average. Within identical conditions, the pressure drop of R245fa is about twice as high as that of R134a.

In the actual industrial production process, with continuous technological progress and process innovation, the factors involved in engineering design become more complex and diverse. Heat exchangers play a crucial role in industrial production as important heat transfer equipment. Among

these factors, the spatial arrangement of heat exchangers is significant as it can directly impact the heat transfer efficiency of the heat exchanger and the overall structure performance. Vertical spatial structures, in certain situations, not only enable more effective use of space but also effectively counteract the gravitational effects that may arise in horizontal arrangements. Vertical orientation can also reduce pipeline length, lower fluid resistance in the pipeline, and improve heat transfer efficiency. Moreover, the vertical arrangement contributes to the uniform distribution of thermal loads, aiding in ensuring that the heat exchanger surfaces are fully engaged in the heat transfer process, thereby improving the overall energy utilization efficiency of the system. Existing research has indicated significant differences in boiling heat transfer characteristics in the tubes between vertical and horizontal flow orientations. Abadi et al. [9] studied the flow boiling heat characteristics of R245fa using a 3 mm inner diameter stainless steel round pipe. The above results demonstrate that under the same working conditions, vertical flow can transition to annular flow earlier, the heat transfer coefficient is higher for vertical flow, while also resulting in a lower pressure drop. Mohseni et al. [10] and Zakaria et al. [11] investigated the flow patterns in various flow directions and found that under experimental conditions, all flow patterns for vertical downward flow, the flow belong to annular flow.

Simultaneously, in the study of phase-change heat transfer characteristics of organic working fluids, it has been found that the reason for the large volume requirement of the heat exchanger is the significant difference in the heat transfer coefficient during phase change. Some researchers have found that techniques such as increasing nucleation sites on the heat transfer surface and enlarging the heat exchange surface area can effectively address this issue [12-15]. Some scholars utilize spherical copper particles, dendrite copper powder, and copper woven tape to create the sintering layer. The results indicate a significant enhancement in heat transfer [16-18].

Tang et al. [19] used supercooled and saturated deionized water under atmospheric pressure as the working fluid. They utilized microfabrication techniques to create an interconnected microchannel network for enhanced pool boiling heat transfer. The experiment showed that these structures have higher nucleate boiling heat transfer coefficient (HTC). Choi et al. [20] used the impregnation method to coat a self-assembled monolayer of octadecyl trichlorosilane branched isomers onto a rectangular glass pipe with the hydraulic diameter of 500  $\mu\text{m}$  for comparative experiments. As the experiment results proved that the heat transfer coefficient of the experimental tube is approximately 1.6 times higher than that of the smooth pipe. Bottini et al. [21] utilized the chemical vapor deposition (CVD) method to coat the inner wall of stainless-steel tubes with a layer of polytetrafluoroethylene acrylate. In comparison to uncoated microtubes, the heat transfer coefficient of the coated tubes increased by 61%. Yang et al. [22] carried flow boiling experiments using organic working fluids in vertical carbon steel tubes. According to the experimental findings, it was revealed that the heat transfer coefficient for the porous tube ranges from 1.8 to 3.5 times the value for the smooth tube. Moreover, the friction pressure drop in the porous tube is within a range of 1.1 to 2.9 times that experienced by the smooth tube. Deng et al. [23] designed and developed porous structures with reentrant cavities (PS-RC) for pool boiling cooling systems. The experiments showed that when water and ethanol were employed as working fluids, during the initial stage of nucleate boiling, the porous structure not only significantly reduced the wall superheat, but also increased the heat transfer coefficients for pool boiling by a factor of 3 and 5.3, respectively.

Nevertheless, there exists a scarcity of experimental studies that comprehensively consider both aspects: the spatial flow direction and the effect of adding porous coatings on the flow boiling of

R245fa. Coupled with today's era-defining challenges such as energy shortages and low utilization efficiency, there is an urgent need for breakthroughs in research in this area. In previous study, our research team carried out experimental studies on the flow boiling performance of R245fa in the horizontal direction using micro/nano-porous coated enhanced tubes. The experimental results revealed a substantial enhancement in heat transfer characteristics on the micro/nano-porous coated surface, with the maximum boiling heat transfer coefficient reaching 3.15 times that of the smooth tube [24]. Therefore, this study continues to use the micro/nano-porous coated tubes. However, the distinction from previous experiments lies in the investigation of boiling heat transfer characteristics under vertical downward flow conditions. The purpose is to explore the factors influencing the enhancement of heat exchanger performance when vertically arranged. The preparation of the micro/nano-porous coated surface in this study mainly involves the formation of a sintered electroplating layer on the inner wall of the tube, through a combination of high-temperature sintering and electroplating processes, resulting in a micro/nano-porous coating. Commercially available spherical copper powder with a purity exceeding 99.5% and a particle size ranging from 130 to 150  $\mu\text{m}$  is used. During the sintering process, particles connect with each other and with the surface, forming sintered necks between them. The electroplating processes enable ions to precipitate in the form of nanoscale particles from the solution, enhancing the bond strength between the surface and substrate. Thereby resulting in a post-plating surface with excellent adhesion strength and hardness, making the surface coating highly resistant to damage. This research not only effectively enhances heat transfer efficiency in ORC systems, thereby improving the overall system efficiency, but also plays a crucial role in the utilization of geothermal resources, waste heat recovery, and solar collectors.

## **2 Experimental system**

### **2.1 Experimental setup**

Building upon the previous research on the horizontal heat transfer characteristics experimental setup, the experimental apparatus has been optimized and upgraded [24]. A rotatable bracket was designed and added to the experimental section, allowing the flow direction of the working fluid to transition from horizontal to vertically downward. The system schematic and the system diagram are illustrated in Fig. 1, respectively. The system is primarily composed of the following four subsystems.

The working fluid cycle system employs a cyclic process with R245fa serving as the working fluid. The principal cycling procedure can be outlined as follows: the working medium from the fluid reservoir first enters the strainer, then, it is diaphragm-pumped into the pressure stabilization tank. It then enters the reheater via a mass flowmeter. And then enters the preheating section of the experimental apparatus. Subsequently, it enters the experimental section for the second heat exchange. Then, the working fluid is cooled in the condenser and finally enters fluid reservoir to complete a cycle. The flow control in the system is primarily regulated by the pump and the bypass control valve.

The working fluid heating system is powered by a couple of DC power respectively. The DC power supplies regulate the output power of the preheating section and the experimental section through independently manipulating the adjustment knobs to tune the heating capacity and conform to experimental prerequisites. Additionally, to enhance the insulation performance of the experimental setup, reduce heat diffusion, and minimize experimental errors caused by radiation heat transfer, the preheating section and experimental section of the apparatus are enveloped with 5 cm thick ceramic fiber insulation and radiation-proof rubber strips.

The cooling system primarily utilizes circulating cooling water inside the condenser to cool the R245fa vapor. The cooling of the circulating water relies on the air-cooled chiller. The cooling water is consistently held at an inlet temperature of 15 °C.

The data measurement system mainly consists of thermocouples and pressure sensors. The K-type thermocouple is used to measure the fluid temperature inside the tube, and the Omega-type thermocouple is used to measure the temperature of experiment section's tube wall. Pressure sensors are used to measure the pressure. The collection of experimental data is performed by the Advantech-417/4118 system from Advantech. The sampling period is 1 second.

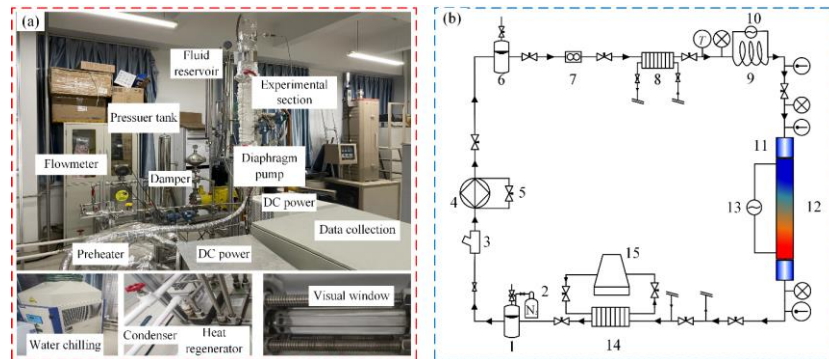


**Figure 1: Experimental system: (a) physical diagram; (b) schematic diagram.**

## 2.2 Experimental section

The experimental section is composed of two segments: the experimental test section and the stream pattern observation section. A stainless-steel tube, characterized by its 10 mm inner diameter, 2 mm wall thickness, and total length of 820 mm, constitutes the experimental test section. The section for observing flow patterns incorporates a pair of quartz glass tubes. These three segments are interconnected by means of flanges. Fig. 2(a) is the structural diagram of the experimental tube. For the purpose of achieving accurate temperature measurements in the experimental section, 27 omega-type thermocouples are securely affixed to the surface of the heat exchange tube along its axial line by using high-temperature-resistant adhesives and insulating tape at nine different temperature measurement cross-sections ( $T_1$ - $T_9$ ). As depicted in Fig. 2.

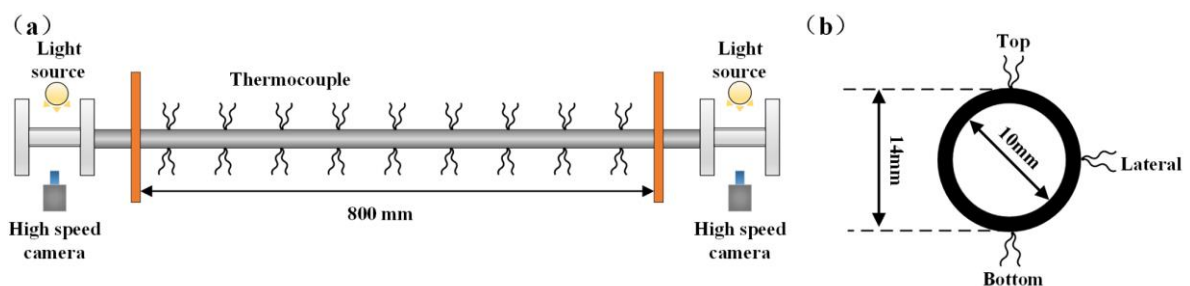


**Figure 2: Experimental test section: (a) structure diagram of the experimental section; (b) circumferential arrangement diagram of the thermocouple.**

## 2.3 Microstructure preparation

Stainless steel tubes are treated by a combination of sintering/plating to build up a sintered layer on the inner wall of the stainless-steel tube. The preparation process and microstructure are shown in Fig. 3.

As shown in the fig.3 from (a-d), the copper powder particles were firstly adhered to the inner wall of the tube using an adhesive; Subsequently, sintering was used to make the copper powder bonded on the surface of the stainless steel, and the sintering was done by using a GSL1200X tube furnace. And then the cooled stainless-steel tubes were taken out for plating, the cathode of the DC

power supply was connected to the stainless-steel tubes, and the anode was connected to the copper rods, and the plating was carried out for 1h under a current density of  $0.05 \text{ A/cm}^2$ . Thus, one can fabricate an enhanced tube with micro/nano-porous coating. Fig. 3(e-h) show the microscopic morphology diagrams of the smooth tube surface, sintered tube surface, sintering/plating tube surface, and the copper powder particles with nano copper electrodeposition structure of the enhanced tube coating.

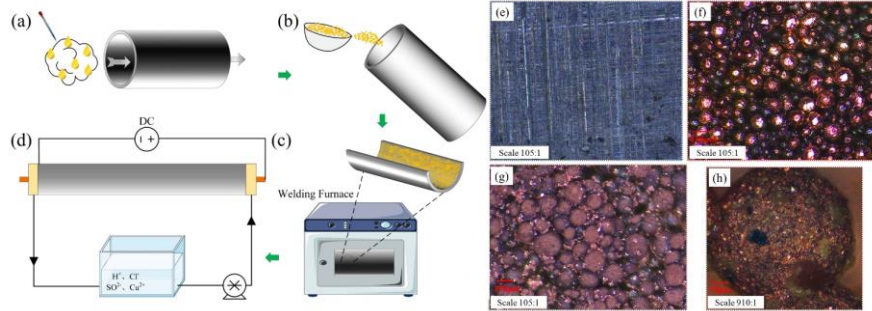


**Figure 3: Surface preparation process and microscopic morphology**

### 2.4 Experimental verification

To ensure the stability of the experiment and the reproducibility of the experimental procedures, deionized water was used to investigate the thermal efficiency of the power source, followed by conducting repetitive experiments. In the repeatability experiment, the boiling temperature of the fluid is assessed under identical working conditions at various time intervals, showing minimal fluctuations, with the range varying between  $0.1 \text{ }^\circ\text{C}$  and  $0.3 \text{ }^\circ\text{C}$ . In the two-phase verification experiment, tests were conducted using R245fa as the working fluid in the smooth tube. The experimentally measured heat transfer coefficient for flow boiling aligns well with the correlations proposed of Wattelet et al. [25] and Fang et al.[26]. The  $e_A$  values were 23.65% and 10.04%, respectively. These are considered suitable for the flow boiling heat transfer. The validation experiment mentioned above demonstrates that the reliability and stability meet the requirements for the experiment.

## 3 Data processing and error analysis

### 3.1 Heat flux density

The preheating section and the experimental section utilized direct current power for heating. The calculation of heat flux ( $q$ ) is as shown in Eq. 1.

$$q = \frac{U_{eva} I_{eva} \eta_{eva}}{\pi d_i L} \quad (1)$$

where ( $d_i$ ) is the inside diameter of the pipe, m; ( $L$ ) is the valid heating length of the experimental section, m; ( $\eta_{eva}$ ) is the evaporator thermal efficiency.

### 3.2 Heat transfer coefficient

Equation (2) provides the computation for the total heat transfer coefficient ( $h$ ) pertaining to the experimental section.

$$h = \frac{q}{T_{w,in,ave} - T_{f,ave}} \quad (2)$$

$$T_{w,in,ave} = T_{w,out,ave} - \frac{qd_i}{2\lambda_w} \ln \frac{d_o}{d_i} \quad (3)$$

$$T_{w,out,ave} = \frac{1}{27} \sum_{j=1}^{27} T_{w,out,j} \quad (4)$$

$$T_{f,ave} = \frac{T_{f,in} + T_{f,out}}{2} \quad (5)$$

where  $d_o$  is the external diameter of the experimental tube,  $T_{f,ave}$  represents the average temperature of the fluid;  $T_{w,in,ave}$  indicates the average temperature of the internal face of the tube;  $T_{w,out,ave}$  indicates the average temperature of the outer wall of the tube;  $T_{w,out,j}$  denotes the temperature at each measurement point on the outer wall of the pipe;  $K$ ,  $\lambda_w$  is the heat conductivity coefficient of the experimental tube,  $\text{Wm}^{-1}\text{K}^{-1}$ ;  $T_{f,in}$  and  $T_{f,out}$  are the inlet and outlet temperatures of the experimental section.

### 3.3 Vapor quality

Formulas (7) and (9) provide the calculation formulas for the vapor quality at the inlet and outlet of the experimental section.

$$H_{eva,in} = H_{pre,in} + \frac{U_{pre} I_{pre} \eta_{pre}}{m_r} \quad (6)$$

$$x_{eva,in} = \frac{H_{eva,in} - H_{eva,in,l}}{H_{eva,in,lg}} \quad (7)$$

$$H_{eva,out} = H_{eva,in} + \frac{U_{eva} I_{eva} \eta_{eva}}{m_r} \quad (8)$$

$$x_{eva,out} = \frac{H_{eva,out} - H_{eva,out,l}}{H_{eva,out,lg}} \quad (9)$$

where  $m_r$  is the mass flow rate of the actuating medium,  $\text{kg}\cdot\text{s}^{-1}$ ;  $H_{pre,in}$  is the enthalpy of the inlet of the actuating medium in the preheating section,  $\text{J}\cdot\text{kg}^{-1}$ ;  $H_{eva,in}$  and  $H_{eva,out}$  are the enthalpies at the inlet and outlet in the experimental section,  $\text{J}\cdot\text{kg}^{-1}$ ;  $H_{eva,in,l}$  and  $H_{eva,in,lg}$ ,  $H_{eva,out,l}$  and  $H_{eva,out,lg}$  are the enthalpy of saturated liquid and latent heat of evaporation at inlet and outlet pressures of the experimental section, respectively,  $\text{J}\cdot\text{kg}^{-1}$ .

### 3.4 Pressure drop

Formula (10) presents the calculation formula for pressure drop.

$$\Delta P_f = \Delta P_{total} - \Delta P_g - \Delta P_a \quad (10)$$

where  $\Delta P_{total}$  is the overall pressure drop, kPa;  $\Delta P_f$  is friction pressure drop, kPa;  $\Delta P_g$  is the gravitational pressure drop, kPa;  $\Delta P_a$  is the acceleration-induced pressure drop, kPa.

### 3.5 Uncertainty analysis

During the experiment, the parameters assessed can be divided into two categories: those measured directly and those determined indirectly. Direct measurement parameters can be directly measured using sensors, such as temperature, pressure, etc. Indirect measurement parameters are calculated based on relevant formulas, including heat transfer coefficients, heat flux density, vapor quality, etc. In the course of the experiment, the operating pressure at the entry point of the experimental section is maintained at approximately 0.6 Mpa. And the mass fluxes ( $G$ ) is between 199.68 and 701.81  $\text{kg}\cdot\text{m}^{-2}\cdot\text{s}^{-1}$ , the inlet vapor quality ( $x_{in}$ ) is 0.01~0.9, and the heat flux ( $q$ ) was controlled at 4.99~74.96  $\text{kW}\cdot\text{m}^{-2}$ . The uncertainty of the indirectly measured parameters and the error values of the conclusions were calculated using the error transfer function. The maximum relative

uncertainty of indirect measurement parameters  $G$ ,  $x$ ,  $h$  and  $q$  is 3.67%, 5.95%, 5.64% and 4.70%, respectively. The error values of the conclusions are represented as error bars in the figure.

## 4 Experimental Results Analysis and Discussion

### 4.1 Visualization Analysis of Flow Patterns

Fig. 4 shows the observed flow patterns in the experiment. For vertical downward flow, both smooth tubes and micro/nano-porous coated tubes exhibit only two flow patterns: annular flow (indicated by A), where the liquid phase surrounds the tube wall, and the central region is occupied by high-speed vapor phase; and dry out flow (indicated by D), where the liquid film on the tube wall ruptures or evaporates, and the vapor phase comes into contact with the tube wall. Under the experimental conditions, except in cases of extreme dry out, the flow regime remains annular, regardless of variations in vapor quality and mass fluxes, which is consistent with similar findings documented in the existing literature [27]. This is mainly attributed to the combined effects of gravity and vapor-liquid interface shear stress promoting the flow of the liquid phase.

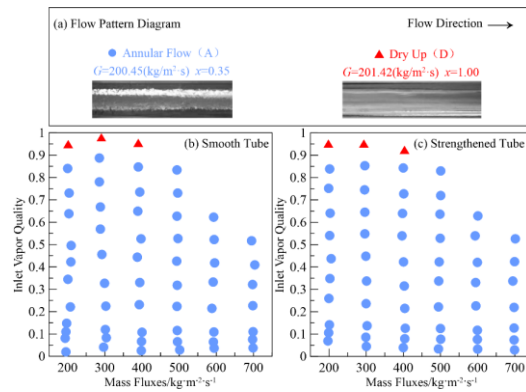


**Figure 4: Flow pattern comparison diagram**

### 4.2 Effect of inlet vapor quality on flow boiling characteristics

Fig. 5 depicts the representation of the effect of inlet vapor quality on the heat transfer coefficient and frictional pressure drop. From Fig. 5 (a), it can be observed that both the smooth tube and the experimental tube exhibit a similar trend in heat transfer coefficient, increasing initially and then decreasing with the increase in inlet vapor quality. At lower vapor quality, nucleate boiling dominates, with bubble agitation contributing to an increase in the heat transfer coefficient. With further increases in inlet vapor quality, the droplets and vapor carried by the high-speed central vapor flow in the tube impact the liquid film on the internal surface of the tube, accelerating the drying process of the film. At this point, convective heat transfer by the vapor phase becomes dominant, leading to a decrease in the heat transfer. Overall, the heat transfer coefficient of the experimental tube outperforms that of the smooth tube. On one hand, the porous structure of the micro/nano-porous coated tube exhibits strong adsorption capabilities for liquid, accelerating wall wetting and promoting more liquid attachment to the inner wall, thereby enhancing boiling heat transfer. For another, the porous structure on the inner wall of the micro/nano-porous coated tube provides numerous nucleation sites, facilitating the prompt detachment of liquid after bubble formation, reducing thermal resistance, and improving heat transfer efficiency. Fig. 5 (b) illustrates the schematic representation of the impact

of inlet vapor quality on the frictional pressure drop in both the smooth tubes and the experimental tubes. Frictional pressure drop in the experimental tube increases with the rise in inlet vapor quality. In contrast, for the smooth pipe, the frictional pressure drop initially increases and then decreases as the inlet dryness fraction rises. Under the same operating conditions, the frictional pressure drop in the smooth tubes is lower than in the experimental tubes.

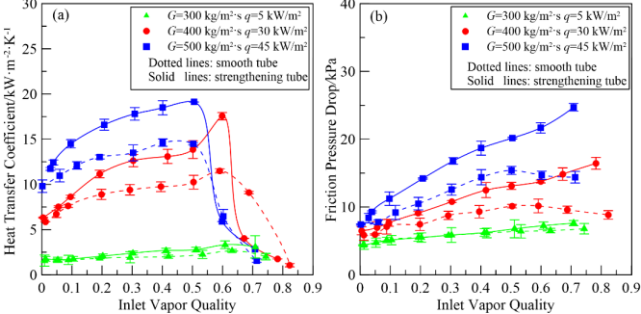


**Figure 5: Influence of inlet vapor quality on flow boiling performance**

**4.3 The Impact of mass Fluxes on Flow Boiling Characteristics**

Fig. 6 illustrates the schematic diagram of the influence of mass fluxes on heat transfer coefficient and frictional pressure drop. From Fig. 6(a), It is clear from the data that with the increase in mass fluxes, the heat transfer coefficient only fluctuates slightly with the increase of mass fluxes, indicating that the influence of mass flux on the heat transfer coefficient is minimal. But it is evident from the graph that under the same mass fluxes, the heat transfer coefficient of the experimental tube is significantly better than that of the smooth tube. This is primarily attributed to the enhanced wetting properties of the inner wall of the experimental tube after treatment, which effectively promotes liquid spreading, accelerates bubble growth, detachment, and release.

From Fig. 6 (b), it can be seen that the frictional pressure drops in both the experimental tube and the smooth tube increase with the rise in mass fluxes. This phenomenon is mainly attributed to the progressive rise in shear forces acting at the pipe wall and the vapor-liquid interface as mass fluxes intensifies, which consequently results in an augmented frictional pressure drop. On the identical operational circumstances, the frictional pressure drop within the experimental tube is notably greater compared to its counterpart in the smooth tube. The main reason lies in the larger capillary forces generated by the porous structure on the inner wall of the experimental tube. As liquid flows downward, influenced by capillary forces, it can penetrate the porous structure more rapidly, generating resistance to the flow. Additionally, the presence of the porous structure itself with a certain thickness reduces the actual size of the pipe, impacting the frictional pressure drop.

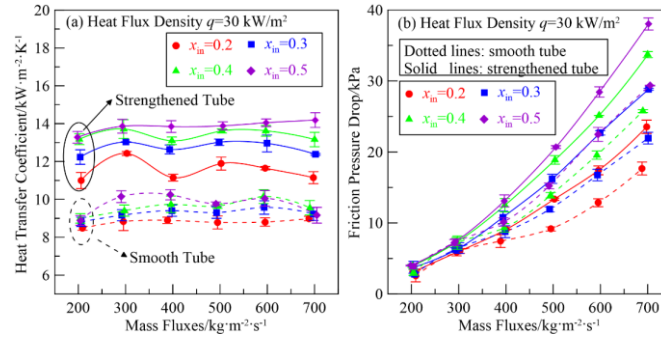


**Figure 6: Influence of mass fluxes on flow boiling performance**

#### 4.4 The Effect of Heat Flux Density on Flow Boiling Characteristics

Fig. 7 (a) is the schematic diagram of the effect of heat flux on heat transfer coefficient. Overall, with the escalating heat flux, the heat transfer coefficients of both smooth and experimental tubes significantly increase. Under the same operating conditions, the heat transfer coefficients of experimental tubes are better than those of smooth tubes. With the increase in heat flux, there is a corresponding rise in the temperature difference on the heated area, which results in the generation of more vaporization nuclei. The increase in the number of vaporization nuclei promotes the generation of more bubbles in the pipeline, which carry away a large amount of heat and lead to an increase in the heat transfer coefficient. Due to the porous structure on the inner surface of the experimental tube, there are more vaporization nuclei compared to smooth tubes, resulting in higher heat transfer efficiency. However, as the heat flux increases further, small bubbles in the tube aggregate into a liquid film attached to the inner wall of the tube. This causes a sudden decrease in the heat transfer coefficient.

Fig. 7 (b) demonstrates the influence of varying heat flux on the frictional pressure drop. It reveals that, for both smooth and experimental tubes, there is no substantial alteration in the frictional pressure drop as the heat flux increases. Meanwhile, due to the strong wettability of the experimental tube surface, the frictional pressure drop inside the smooth tube is lower than that of the experimental tube.

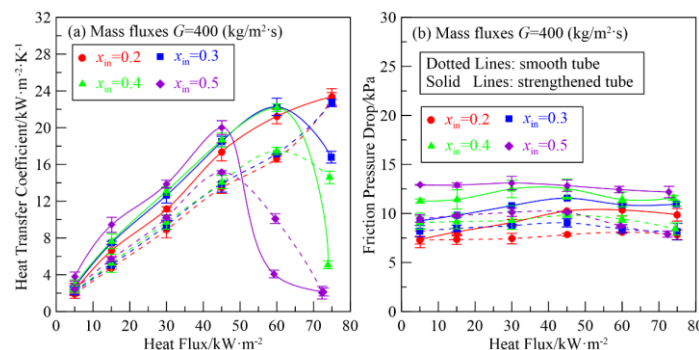


**Figure 7: Influence of heat flux on flow boiling performance**

#### 4.5 Analysis of strengthening mechanism

With the aim of more intuitively demonstrate the heat transfer enhancement characteristics of the experimental tube, the enhanced heat transfer factor (*EF*) and performance evaluation coefficient (*PEC*) are defined.

$$EF = \frac{h_s}{h} \quad (11)$$

$$PEC = \frac{h_s/h}{(\Delta p_{f,s}/\Delta p_f)^{1/6}} \quad (12)$$

where  $h_s$  and  $h$  represent the boiling heat transfer coefficient of experimental tube and smooth tube, respectively;  $\Delta P_{f,s}$  is the friction pressure drop of the experimental tube, kPa.

From Fig. 8 (a) to (b), it can be observed that under various operating conditions, the enhanced heat transfer factor is always above 1. Moreover, with the increase of the inlet vapor quality, the enhanced heat transfer factor generally shows an increasing trend, indicating a pronounced enhancement effect of heat transfer in the experimental tube. As inlet vapor quality increases to a high level, the convective heat transfer of steam plays an important role, leading to a sharp decrease in the enhanced heat transfer factor. Additionally, a high degree of consistency in the trends of the enhancement heat transfer factor and comprehensive evaluation factor is observed in the graph comparison.

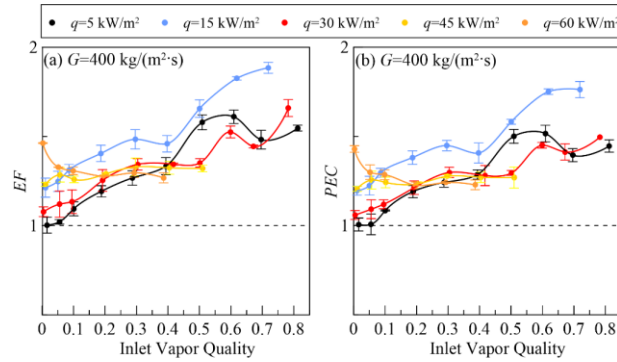


**Figure 8: Effect of inlet vapor quality on enhanced heat transfer and comprehensive evaluation factors.**

#### 4.6 Analysis of Changes in liquid film thickness

Fig. 9 shows the characterization of changes in liquid film thickness at the inlet and outlet of the experimental section. The mass fluxes ( $G$ )  $\approx 100 \text{ kg}\cdot\text{m}^{-2}\cdot\text{s}^{-1}$ ,  $x \approx 0.05$ , the inside diameter of the tube ( $d_i$ ) is 10 mm. The curved portion of the figure is the ratio of the liquid film thickness to the ( $d_i$ ) of the tube, and the change of the liquid film thickness is represented by the value of  $d/d_i$ . The liquid film thickness on both sides of the inlet section is significantly higher than that of the outlet section, and the overall liquid film thickness at the outlet decreases by about 28.6%. For vertical downward flow, where the gravitational direction aligns with the flow direction, it accelerates the downward movement of the working fluid and the rate of diffusion penetration, thereby reducing the liquid film thickness.

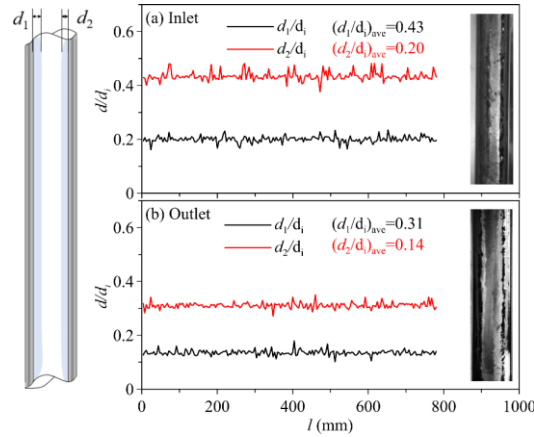


**Figure 9: Changes in inlet and outlet flow patterns of micro-nano porous coated tubes**

With the reduction in liquid film thickness, the increase in liquid phase velocity is due to the constant mass fluxes and inlet vapor quality in the tube. The mass fluxes  $G \approx 100 \text{ kg} \cdot \text{m}^{-2} \cdot \text{s}^{-1}$ ,  $x \approx 0.05$ . The liquid and gas phase velocities are calculated separately. Calculation formula is given by Eq. 12.

$$v = \frac{M}{\rho A} \quad (12)$$

where ( $v$ ) is the velocity,  $\text{m} \cdot \text{s}^{-1}$ ; ( $M$ ) is the mass flow rate,  $\text{kg/s}$ ; ( $\rho$ ) is the density,  $\text{kg} \cdot \text{m}^{-3}$ ; The area ( $A$ ) can be calculated from the total cross-sectional area of the tube and the average thickness of the liquid film. The density ( $\rho$ ) can be found by the physical property software according to the working condition information. The result of the incoming data are as follows: the liquid phase velocity ( $v_l$ ) at the inlet is  $0.0912 \text{ m} \cdot \text{s}^{-1}$ ; the vapor phase velocity ( $v_g$ ) is  $1.0973 \text{ m} \cdot \text{s}^{-1}$ . In the same way, the liquid phase velocity ( $v_l'$ ) at the outlet is  $0.1129 \text{ m} \cdot \text{s}^{-1}$ ; the vapor phase velocity ( $v_g'$ ) is  $0.4966 \text{ m} \cdot \text{s}^{-1}$ . The calculated liquid phase velocity is increased by about 21.9%; the vapor phase velocity is reduced by about 54.8%. In-tube flow boiling heat transfer is mainly the result of the combined effect of nuclear state boiling and convective heat transfer. Establish a flow boiling superposition model inside the tube, taking into account the effects of nuclear state boiling and convective heat transfer on the total heat transfer coefficient. It was analyzed using the Gungor and Winterton [28] correlation. Since the effect of nuclear state boiling is small, the flow boiling heat transfer coefficient enhancement is about 21.4%.

## 5 Conclusion

This study investigates the boiling heat transfer characteristics of R245fa flowing vertically downward within both a micro/nano-porous coated tube and a smooth tube. The conclusions drawn from the research are as follows:

(1) Flow pattern visualization analysis indicates that both enhanced tubes and smooth tubes exhibit only the annular flow pattern, with drying flow occurring at higher inlet vapor qualities.

(2) The porous coating on the inner wall surface of the experimental tube demonstrates excellent rewetting characteristics, effectively facilitating the rapid replenishment of liquid on the heat exchange surface. Micro/nano-porous coated tubes show a substantial improvement in boiling heat transfer, with the maximum enhancement factor reaching 1.88 times that of smooth tubes.

(3) For vertical downward flow, the direction of gravity aligns with the flow direction, which further accelerates the downward movement of the liquid. Additionally, the porous structure enhances the rate of diffusion and penetration of the liquid, resulting in a reduction of the liquid film thickness. Specifically, the liquid film thickness is reduced by approximately 28.6%, leading to a significant

decrease in thermal resistance and thereby improving flow boiling heat transfer. Furthermore, the liquid phase velocity has increased by approximately 21.9%, while the vapor phase velocity has decreased by about 54.8%.

### Acknowledgement:

This work was supported by National Natural Science Foundation of China (51906231), Henan Provincial Association for Science and Technology Youth Talent Support Project(2024HYTP022), Henan Provincial Department of Science and Technology Research Project (242102321098, 232102321091).

### Nomenclature

$d_i$	Internal diameter of the pipeline(m)
$d_o$	Outside diameter of pipe(m)
$h_s$	Enhanced tube heat transfer coefficient
$h$	Smooth tube heat transfer coefficient
$e_A$	Mean absolute deviation
$x_{in}$	Inlet vapor quality
$v_l$	Inlet liquid phase velocity(m/s)
$v_g$	Inlet vapor phase velocity(m/s)
$v_l'$	Outlet liquid phase velocity(m/s)
$v_g'$	Outlet vapor phase velocity(m/s)
$M$	The mass flow rate(kg/s)

### Reference

- [1] Tang, J. P., *ea al.*, An effective method for working fluid design of organic Rankine cycle, *Processes.*, 10(2022), 9, pp.1857.
- [2] Herath, H., M., D., P., *ea al.*, Working fluid selection of organic Rankine cycles, *Energy Reports.*, 6(2020), pp.680-686.
- [3] Chen, T., *ea al.*, Experimental analyses of moderately high-temperature heat pump systems with R245fa and R1233zd(E), *Energy Engineering.*, 119(2022), pp.2231-2242.
- [4] Luo, X., *ea al.*, Experimental investigation on high-temperature flow boiling heat transfer characteristics of R245fa in a horizontal circular tube, *Applied Thermal Engineering.*, 225(2023), pp.120260.
- [5] Dang, C., *ea al.*, Experimental study on saturation pool boiling heat transfer characteristics of R245fa on the surface covered by sintered copper powder, *Case Studies in Thermal Engineering.*, 37(2022), pp.102223.
- [6] Xu, W., *ea al.*, PVTx properties of the R600a/R245fa for low temperature organic Rankine cycle, *The Journal of Chemical Thermodynamics.*, 176(2023), pp.106904.
- [7] Li, C., *ea al.*, An experimental investigation of flow boiling instability of R245fa in a horizontal tube, *Physics of Fluids.*, 35(2023), 8, 084122.
- [8] Al-Hajri, E., *ea al.*, Performance characterization of R134a and R245fa in a high aspect ratio microchannel condenser, *International Journal of Refrigeration.*, 36(2013), pp.588-600.
- [9] Abadi, G., B., *ea al.*, Effect of gravity vector on flow boiling heat transfer, flow pattern map, and pressure drop of R245fa refrigerant in mini tubes, *International Journal of Multiphase Flow.*, 83(2016), pp.202-216.

- [10] Mohseni, S., G., *ea al.*, Flow pattern visualization and heat transfer characteristics of R134a during evaporation inside a smooth tube with different tube inclinations, *International Communications in Heat and Mass Transfer.*, 59(2014), pp.39-45.
- [11] Zakaria, M., I., *ea al.*, An empirical investigation on flow pattern, heat transfer, and pressure drop during flow boiling of R1234yf in an inclined plain tube, *International Journal of Thermal Sciences.*, 170(2021), pp.107100.
- [12] Chen, G., Non-Fourier phonon heat conduction at the microscale and nanoscale, *Nature Reviews Physics.*, 3(2021), 8, pp.555-569.
- [13] Tan, K., *ea al.*, Effect of wettability on flow boiling heat transfer in a microtube, *Case Studies in Thermal Engineering.*, 26(2021), pp.101018.
- [14] Enoki, K., *ea al.*, Water flow boiling heat transfer in vertical mini-channel, *Experimental Thermal and Fluid Science.*, 15(2020), 19, pp.7050.
- [15] Marseglia, G., *ea al.*, Enhancement of microchannel heat sink heat transfer: Comparison between different heat transfer enhancement strategies, *Experimental Thermal and Fluid Science.*, 150(2024), pp.111052.
- [16] Sun, Y., *ea al.*, Flow boiling enhancement of FC-72 from microporous surfaces in minichannels, *Therm. Fluid Sci.*, 35(2011), 7, pp.1418-1426.
- [17] Bai, P., F., *ea al.*, Enhanced flow boiling in parallel microchannels with metallic porous coating, *Applied Thermal Engineering.*, 58(2013), 1-2, pp.291-297.
- [18] He, B., I., *ea al.*, Flow boiling characteristics in bi-porous mini-channel heat sink sintered with copper woven tape, *International Journal of Heat and Mass Transfer.*, 158(2020), pp.119988.
- [19] Tang, Y., *ea al.*, Effect of structural parameters on pool boiling heat transfer for porous interconnected microchannel net, *International Journal of Heat and Mass Transfer.*, 93(2016), pp.906-917.
- [20] Choi, C., *ea al.*, Flow boiling behaviors in hydrophilic and hydrophobic microchannels, *Experimental Thermal and Fluid Science.*, 35(2011), 5, pp.816-824.
- [21] Bottini, J., L., *ea al.*, Influence of wettability due to laser texturing on critical heat flux in vertical flow boiling, *International Journal of Heat and Mass transfer.*, 127(2018), pp.806-817.
- [22] Yang, D., *ea al.*, Experimental studies on the enhanced flow boiling heat transfer and pressure drop of organic fluid with high saturation temperature in vertical porous coated tube, *7th International Symposium on Multiphase Flow.*, 1547(2012), pp.442-453.
- [23] Deng, D., X., *ea al.*, Pool boiling heat transfer of porous structures with reentrant cavities, *International Journal of Heat and Mass Transfer.*, 99(2016), pp.556-568.
- [24] CAO, S., *ea al.*, R245fa flow boiling heat transfer in a sintering and electroplating modulated tube, *Applied Thermal Engineering.*, 219(2022), pp.119459.
- [25] Wattelet, J., P., *ea al.*, Evaporative characteristics of R-134a, MP-39, and R-12 at low mass fluxes, *Ashrae Transactions.*, 100(1993), pp.603–615.
- [26] Fang, X., D., *ea al.*, A general correlation for saturated flow boiling heat transfer in channels of various sizes and flow directions, *International Journal of Heat and Mass Transfer.*, 107(2016), pp.972-981.
- [27] Fang, X., *ea al.*, A general correlation for saturated flow boiling heat transfer in channels of various sizes and flow directions, *International Journal of Heat and Mass Transfer.*, 107(2017), pp.972-981.
- [28] Gungor, K., E., *ea al.*, A general correlation for flow boiling in tubes and annuli, *International*

*Journal of Heat and Mass Transfer.*, 29(1986), 3, pp.351-358.

Submitted: 5.7.2024.

Revised: 13.9.2024.

Accepted: 20.9.2024.